Geomechanics and Engineering, *Vol. 38, No. 3 (2024) 231-247*
https://doi.org/10.12989/gae.2024.38.3.231

An investigation into the effects of lime-stabilization on soil-geosynthetic interface behavior

Khadije Mahmoodi*[1], Nazanin Mahbubi Motlagh[2] and Ahmad-Reza Mahboubi Ardakani[3]

[1]*Department of Civil Engineering, Faculty of Engineering, Ardakan University, P.O. Box 184, Ardakan, Iran*
[2]*School of Civil and Environmental Engineering, UNSW Sydney, NSW, Australia*
[3]*Faculty of Civil, Water and Environmental Engineering, Shahid Beheshti University, P.O. 16765-1719, Tehran, Iran*

(*Received May 9, 2023, Revised July 13, 2024, Accepted July 15, 2024*)

Abstract. The use of lime stabilization and geosynthetic reinforcement is a common approach to improve the performance of fine-grained soils in geotechnical applications. However, the impact of this combination on the soil-geosynthetic interaction remains unclear. This study addresses this gap by evaluating the interface efficiency and soil-geosynthetic interaction parameters of lime-stabilized clay (2%, 4%, 6%, and 8% lime content) reinforced with geotextile or geogrid using direct shear tests at various curing times (1, 7, 14, and 28 days). Additionally, machine learning algorithms (Support Vector Machine and Artificial Neural Network) were employed to predict soil shear strength. Findings revealed that lime stabilization significantly increased soil shear strength and interaction parameters, particularly at the optimal lime content (4%). Notably, stabilization improved the performance of soil-geogrid interfaces but had an adverse effect on soil-geotextile interfaces. Furthermore, machine learning algorithms effectively predicted soil shear strength, with sensitivity analysis highlighting lime percentage and geosynthetic type as the most significant influencing factors.

Keywords: geosynthetic; interaction parameters; interface efficiency; lime stabilization; machine learning

1. Introduction

Construction on clayey soils presents several challenges, including high settlement, poor strength and load-bearing capacity, as well as swelling, and shrinkage. One way to address these challenges is by employing chemical additives. Stabilization of soils with chemical additives, such as lime, improves soils in many ways including strength parameter enhancement, potential mitigation of swelling and shrinkage, plasticity index reduction, and improved durability under various weather conditions (e.g., resistance to freezing-thawing, drying-wetting, erosion, and aeration) (Behnood 2018). Lime, a readily available and affordable additive, has long been considered a popular choice for soil stabilization (Bell 1996, Guney *et al.* 2007, Al-Mukhtar *et al.* 2012, Stoltz *et al*. 2014, Bozbey *et al*. 2018, Sujatha *et al.* 2018, Rastegarnia *et al*. 2020, Okonta and Nxumalo 2022, Ramesh *et al.* 2022). Stabilization of clayey soils induces pozzolanic reactions, leading to agglomeration and reduced plasticity. In general, the lime stabilization of soils has three stages: (1) soil agglomeration, (2) formation of calcite crystals following the reaction between lime and the CO_2 content of the air; and (3) formation of calcium silicate hydrates, calcium aluminate hydrates, and calcium aluminum-silicate hydrate. It should be noted that calcium aluminum-silicate hydrate typically forms at higher lime concentrations (Al-Mukhtar *et al.* 2010, Al-Mukhtar *et al.* 2012, Al-Swaidani *et al.* 2016).

In addition to lime stabilization, geosynthetics, such as geogrids and geotextiles, offer another effective method to address the challenges mentioned earlier. Geosynthetic materials have been utilized for different applications such as improved load-bearing capacity, filtration, drainage, layer separation, and settlement uniformity (Marienfeld 2013, Selvakumar and Soundara 2019, Roodi and Zornberg 2020, Tiwari and Satyam, 2020). Geosynthetics with their high tensile strength and stiffness, provide excellent confinement to soil particles and effectively redistributes applied loads thereby improving the overall stability and ductility of the structure (Marienfeld 2013, Selvakumar and Soundara 2019, Roodi and Zornberg 2020, Tiwari and Satyam 2020). However, the transfer of stresses from the soil to the reinforcement at the interface plays a key role in the performance of the reinforced soil system. Therefore, it is essential to optimize the interaction parameters of soil-geosynthetics interface for evaluation of the shear strength of geosynthetic-reinforced soils. These parameters are dependent on the soil properties including maximum dry unit weight, moisture content, gradation, soil particle size and shape, and also geosynthetic characteristics i.e. geometry and tensile strength (Lopes 2002). Liu *et al.* formulated the shear strength of geogrid-reinforced soils according to Eq. (1) (Liu *et al.* 2009)

$$R_{S+GG} = A.\rho.\tau_{soil} + A(1-\rho)\tau_{S-G} + R_B \quad (1)$$

where A is the total area of the shear box, ρ is the ratio of the geogrid opening area to the total shear area, τ_{S-G} is the soil-geosynthetic interface shear resistance, τ_{soil} is the soil shear resistance and R_{S+GG} and R_B are the total shear strength of reinforced samples and the strength of the

*Corresponding author, Assistant Professor
E-mail: mahmoodi@ardakan.ac.ir

ISSN: 2005-307X (Print), 2092-6219 (Online)

transverse ribs, respectively. The bearing resistance ratio ,β, also represents the contribution of transverse ribs in total shear strength of geogrid-reinforced specimens and can be defined based on Eq. (2) (Liu *et al.* 2009)

$$\beta = (R_{S+GG} - A.\rho.\tau_{soil} - A(1-\rho)\tau_{S-G})/R_{S+GG} \quad (2)$$

Cowell defined interface efficiency, C_i, as the ratio of the mobilized shear strength in the soil-reinforcement interface to the soil shear strength and is calculated based on Eq. (3) (Cowell 1993)

$$C_i = (C_a + \sigma_n tan\delta)/(C + \sigma_n tan\varphi) \quad (3)$$

where C_a and δ are the cohesion and friction angle of the soil-reinforcement interface, respectively. Moreover, C is the soil cohesion, φ is the internal friction angle, and σ_n is normal stress. C_i value larger than 1 represents an effective soil-geosynthetic interaction, i.e., the soil-reinforcement interface strength is greater than the soil shear strength. Furthermore, C_i smaller than 0.5 implies a poor soil-geosynthetic interaction (Tatlisoz *et al.* 1998). Abu-Farsakh et al. reported that C_i would be typically greater than 0.7 for clayey soils, suggesting good binding between clayey soils and geogrids. A rise in the moisture content and/or a reduction in the dry density would diminish the interface efficiency (Abu-Farsakh *et al.* 2007).

While clay stabilization is a popular method for remediating cohesive soils, it cannot effectively address all geotechnical challenges (Tang *et al.* 2007, Tiwari and Satyam 2020). For example, although lime stabilization enhances soil strength, it can also increase brittleness (Cai *et al.,* 2006, Wang *et al*. 2013). To overcome these limitations, lime-stabilized soils can be reinforced with geogrids and geotextiles to improve their ductility and stability (Porbaha 1996, Jahandari *et al*. 2019, Roodi and Zornberg 2020). By combining soil stabilization and reinforcement, the soil resists compressive stresses while the geosynthetics handle tensile stresses.

Several studies support the effectiveness of combining lime stabilization with geosynthetic reinforcement. According to results of centrifuge tests, Porbaha (1996) reported that geotextile reinforcement in lime-treated retaining walls enhanced their stability and flexibility. Similarly, other researchers conducted centrifuge testing combined with numerical analysis and discovered that incorporating a geogrid reinforcement layer improved the stability of quay walls filled with lime-treated fine-grained soils (Ye *et al*. 2012). Using the results of unconfined compressive tests, Jahandari *et al*. (2019) reported that while lime stabilization changes ductile soil behavior to brittle, geogrid-reinforced soil exhibits semi-ductile behavior. Additionally, Roodi and Zornberg reported that geosynthetics significantly reduces the width of longitudinal road cracks on swelling clay, whereas lime stabilization alone worsens these cracks due to subgrade volume variations (Roodi and Zornberg 2020). Despite the successful application of lime-stabilized reinforced soils in geotechnical constructions, a key challenge remains regarding the evaluation of interaction parameters and interface efficiency for the soil-geosynthetics interface.

Traditionally, soil shear strength has been determined through various tests like direct shear testing, triaxial testing, and pull-out testing, which are highly accurate but time-consuming and expensive. This highlights the need for faster and more cost-effective methods for evaluating soil shear strength. To address this challenge Machine Learning (ML) offers a promising solution, with effective algorithms like Support Vector Regression (SVR) and Artificial Neural Networks (ANNs) demonstrating the ability to accurately estimate soil strength parameters in a shorter timeframe and at lower costs. The generalization of these models allows them to be applied in various scenarios, providing valuable insights for engineers. Furthermore, ML implementation can reduce the need for extensive laboratory testing while still providing reliable estimates. ML has already been successfully applied to various geotechnical problems, including swelling pressure estimation (Jalal *et al.* 2021), uniaxial compressive strength prediction (Suman et al., 2016, Jalal *et al.* 2021, Tabarsa *et al*. 2021), and soil elasticity modulus estimation (Ghanizadeh *et al*. 2022).

Several studies have explored SVR and ANNs for soil shear strength evaluation (Armaghani *et al*. 2020, Dinarvand and Ardakani 2022, Lin *et al*. 2022). Additionally, Pramanic *et al*. (2022) demonstrated the effectiveness of the ANN-based response surface method for assessing the reliability of geosynthetic reinforced retaining walls (Pramanik *et al.* 2022).

While existing research has explored lime stabilization and geosynthetic reinforcement of clay soils, a critical gap remains in the understanding of interface behavior in stabilized-reinforced soils. This study addresses this gap by evaluating, for the first time, the interface efficiency and interaction parameters of lime-stabilized cohesive soil/geosynthetics at varying lime percentages and curing ages using direct shear testing. Additionally, the soil shear strength is estimated using both Support Vector Machine (SVM) and Artificial Neural Network (ANN) algorithms.

2. Materials and methods

Low-plasticity clayey soil was collected from the south of Tehran, Iran and its properties are listed in Table 1. The chemical composition of hydrated lime, provided by the manufacturer, is presented in Table 2. Similarly, manufacturer specifications for the geogrids and geotextiles are provided in Tables 3 and 4, respectively. Two geogrids (GG1 and GG2) with varying aperture sizes and two geotextiles (GT1 and GT2) with different tensile strengths are employed in this study. Fig. 1 plots the compaction curves of the unstabilized clay and lime-stabilized clay with different lime contents. The compaction test indicates that a rise in the lime content reduces the maximum dry unit weight and increases the optimum moisture content (OMC). This result is consistent with another work which reported that the dry unit weight reduction was due to the specific density difference between clay and hydrated lime. Since lime required water for the pozzolanic reaction, an increase in the lime concentration raised the OMC (Saeed *et al*. 2015).

The specimens were divided into four groups:

- Natural soil (unstabilized-unreinforced specimens)
- Soils stabilized with different lime percentages

Table 1 Soil properties

Parameter	value
Liquid limit (%)	28.3
Plastic limit (%)	17
Plasticity index (%)	11.3
Gs	2.58
γ_{dmax} (kN/m^3)	18.3
ω_{opt} (%)	15.3
C (kPa)	27.5
$\varphi°$	24.8

Table 2 Chemical composition of lime

Oxide	CaO	SiO_2	Fe_2O_3	Al_2O_3	MgO	SiO_3	CO_2	H_2O
Quantity (%)	72.8	0.5	0.1	0.2	0.4	0.45	2.2	22.4

Table 3 Geogrid properties

Properties	GG1	GG2
Apparent size (mm)	4×4	10×10
Tensile strength (kN/m)	10	6
Elongation at failure (%)	11	11
Area of longitudinal ribs (cm^2)	6	3
Area of transverse ribs (cm^2)	6	3
Percent open area (%)	67	83
Thickness of ribs (mm)	2	2
Tensile strength at 1% elongation (kN/m)	2	1.2
Tensile strength at 2% elongation (kN/m)	3.5	2.1
Tensile strength at 5% elongation (kN/m)	7	4.2
Weather resistance (Class)	high	high
Reduction factor for creep rupture for 120 years	1.46	1.46
Reduction factor for mechanical damage	1.18	1.18
Reduction factor for chemical and biological effects	1.03	1.03

Table 4 Geotextile properties

Properties	GT1	GT2
Geotextile type	Nonwoven	Nonwoven
Fiber type	Polyester	Polyester
Tensile strength (kN/m)	5.5	12
Mass per unit area (g/m^2)	200	400
Thickness (mm)	1.5	3
Elongation at failure (%)	55	55
Permeability (cm/s)	0.23	0.23
CBR puncture resistance (kN/m)	2.5	3.4
Cone drop (mm)	6	6

(2%, 4%, 6%, and 8%) at curing ages of 1, 7, 14, and 28 days (stabilized-unreinforced specimens);

- Soils reinforced with a geosynthetic (unstabilized-reinforced specimens); and
- Soils stabilized with different lime percentages (2%, 4%, 6%, and 8%) and reinforced with geosynthetics at curing ages of 1, 7, 14, and 28 days (stabilized-reinforced specimens).

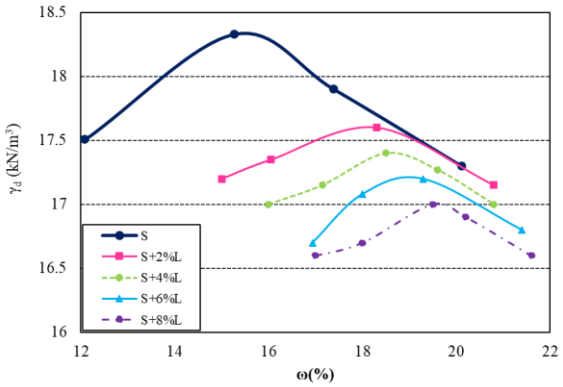

Fig. 1 Standard Proctor tests results

Fig. 2 Direct shear apparatus photo

To stabilize unreinforced clay, dry clay was mixed with different lime percentages (2%, 4%, 6%, and 8%). Water was then added, based on the OMC obtained from the standard Proctor test, to the clay-lime mixture. The obtained mixture was placed within the direct shear box in three layers to be compacted to the maximum dry unit weight. Then, the soils were demolded and placed within a plastic bag to be cured for 1, 7, 14, and 28 days. The direct shear test was carried out at a rate of 1 mm/min and normal stresses of 100, 200, and 400 kPa under a strain-control load. To evaluate the shear strengths of the specimens, the direct shear test was implemented based on ASTM D-3080 with a 6 × 6 cm^2 box (Fig. 2). The direct shear test is the most efficient test to measure the soil-geosynthetic interaction parameters when the soil mass slides on the reinforcement.

The direct shear test for reinforced samples was conducted following ASTM D-5321. The lower half of the shear box was filled with half of the clay-lime-water mixture (at the OMC) and compacted to the maximum dry unit weight, as shown in Fig. 3. A single layer of geosynthetic (geotextile or geogrid) was then placed in the gap between the upper and lower shear boxes. The geosynthetic layer should be flat and free of any folds, wrinkles, or stretching. It should also be in complete contact with the entire test area. To prevent movement during shearing, geosynthetic clamping devices were used to fix the geosynthetics layer in place. The upper shear box was then placed and filled with the remaining half of the mixture

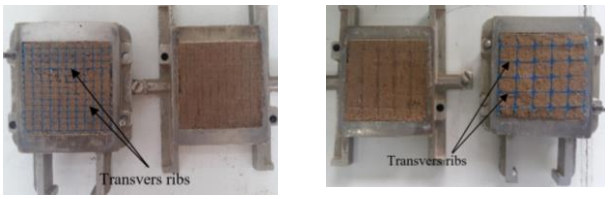

(a) Reinforced with GG1 (b) Reinforced with GG2

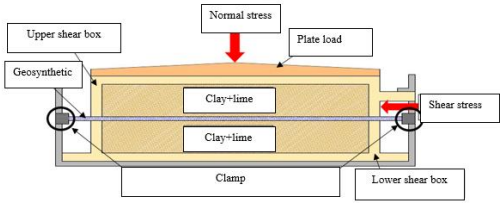

(c) Schematic figure of shear box

Fig. 3 Reinforced specimens in direct shear test

using the same compaction procedure. The cured specimens were placed in the shear machine with the reinforcement fixed to avoid sliding and shear folding. The shear load was applied at a rate of 1 mm/min under normal stresses of 100, 200, and 400 kPa.

3. Results and discussion

3.1 Effect of lime stabilization on shear strength of unreinforced soil

Fig. 4 plots the direct shear strength of the stabilized-unreinforced specimens at curing ages of 1, 7, 14, and 28 days. As can be seen, the shear strength of the specimens increases with the curing age and normal stress. Furthermore, the optimal lime percentage is found to be 4%. It should be noted that earlier works reported an optimal lime percentage to be 5% (Cai *et al.* 2006, Al-Mukhtar *et al*. 2010, Abdi *et al.* 2021). Exceeding the optimal lime content actually reduces soil shear strength. Several mechanisms likely contribute to this phenomenon, particularly in silica-rich clays. Literature suggests potential roles for excess lime acting as a lubricant between soil particles (Bell 1996), the presence of platy unreacted lime particles hindering strength gain (Kumar *et al*. 2007), and the development of highly porous cementitious gel upon excessive lime addition (Dash and Hussain 2012). This gel, despite some cementation benefits, creates significant porosity, weakening the overall soil structure. The interplay of these factors with increasing lime content likely leads to the observed decrease in overall strength. The optimal lime percentage is dependent on the clay type, clay minerals, and lime type. A sub-optimal lime content will not sufficiently alkalinize the soil, hindering the complete dissolution of silicate and aluminate. As a result, cementation and strength will not be maximized. It is also observed that the shear strength values of the specimens at a lime content of 4% and a curing age of 28 days are 490%, 345%, and 244% higher than those of the unstabilized-unreinforced specimens under normal stresses of 100, 200, and 400 kPa, respectively.

3.2 Effect of reinforcement and stabilization on shear strength

Fig. 5 depicts the direct shear strength of the geogrid-reinforced/lime-stabilized soil (with transverse ribs) at different lime contents. A comparison of Figs. 4 and 5 demonstrates that the geogrid-reinforced/lime-stabilized specimens have higher shear strength values than the unstabilized-unreinforced specimens under given normal stresses. For example, the GG1- and GG2-reinforced/unstabilized soils have 94% and 54% higher shear strength than the unstabilized-unreinforced soil at a normal stress of 400 kPa. This strength enhancement is attributed to the interlocking of soil particles in geogrid apertures and the additional strength arising from transverse ribs. Lime stabilization has a greater contribution than geogrid reinforcement to the shear strength enhancement.

This is evident from the shear strength of the stabilized-unreinforced specimen at a 4% lime content and a curing age of 28 days, which is almost 220%, 140%, and 77% higher than that of the GG1-reinforced specimen at normal stresses of 100, 200, and 400 kPa, respectively. The relative contribution of lime stabilization compared to geogrid reinforcement diminishes with increasing normal stress. This is because the main mechanism for strength enhancement in reinforced soil is the increased friction angle, which is directly proportional to the normal stress (σ) in the Mohr-Coulomb model ($\tau = c + \sigma \tan \varphi$). In contrast, lime stabilization primarily improves shear strength through enhanced cohesion. Furthermore, consistent with this observation, GG1 reinforcement leads to a greater shear strength improvement compared to GG2. This demonstrates that geogrids with smaller aperture sizes are more efficient in fine-grained soils.

Results from Figs. 4 and 6 show that reinforcing soil with geotextiles increases the shear strength of the GT1 and GT2-reinforced soils about 59% and 84% in comparison to unstabilized-unreinforced specimens under a normal stress of 400 kPa, respectively. The geotextile with greater tensile strength, results in a greater increase in shear strength. Geogrids outperform geotextiles in reinforcement, as evidenced by Figs. 5 and 6. Eq. 1 explains this advantage. Geogrids improve shear resistance through three mechanisms: 1) confining soil particles to maximize friction between them, 2) distributing stress more evenly with their stiff ribs to reduce stress concentration, and 3) mobilizing shear stresses at the soil geogrid interface. This translates to a tensile force within the geogrid, ultimately enhancing the total shear resistance of soil-geosynthetic system, which aligns with findings from previous studies (Bergado *et al.* 1993, Liu *et al.* 2009).

Fig. 7 investigates the impact of lime stabilization and geosynthetic reinforcement on shear strength under a normal stress of 400 kPa. It compares the shear strength of unstabilized specimens (both reinforced and unreinforced) with stabilized specimens (both reinforced and unreinforced). Notably, curing a soil sample with 4% lime for 28 days resulted in a remarkable 244% increase in shear strength compared to an unstabilized-unreinforced sample.

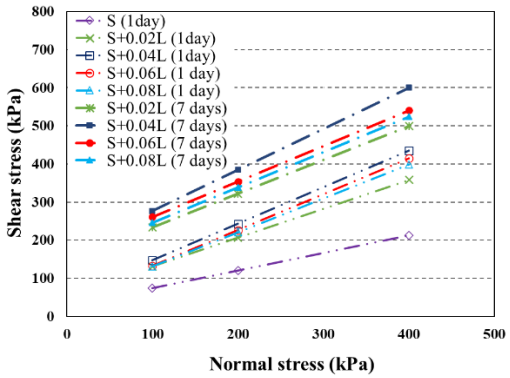

(a) Curing ages of 1 and 7 days

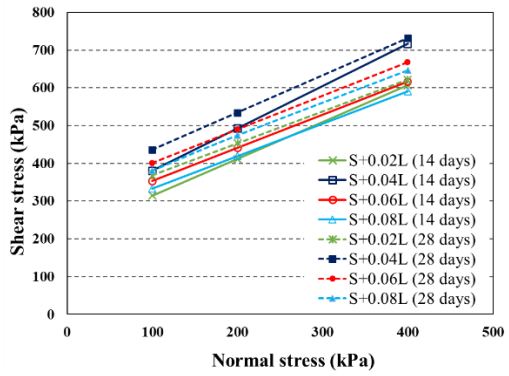

(b) Curing ages of 14 and 28 days

Fig. 4 Shear strength of unreinforced soils (lime stabilized and unstabilized)

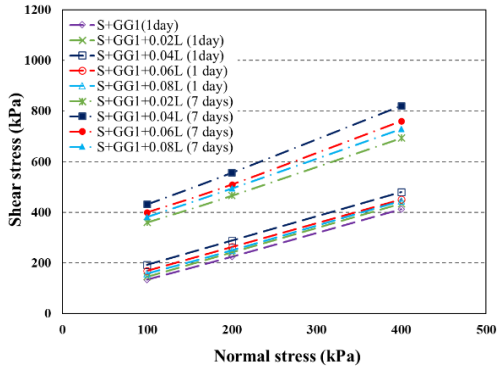

(a) GG1-reinforced at curing ages of 1 and 7 days

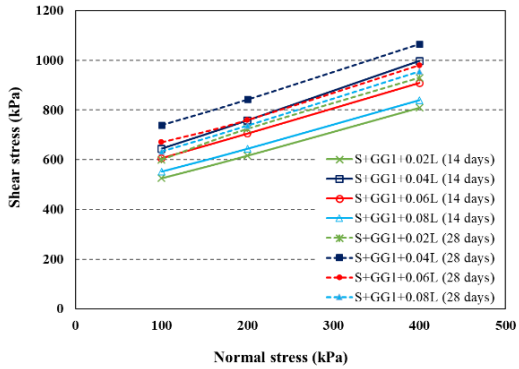

(b) GG1-reinforced at curing ages of 14 and 28 days

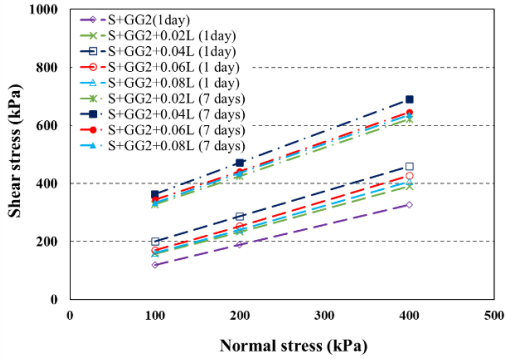

(c) GG2-reinforced at curing ages of 1 and 7 days

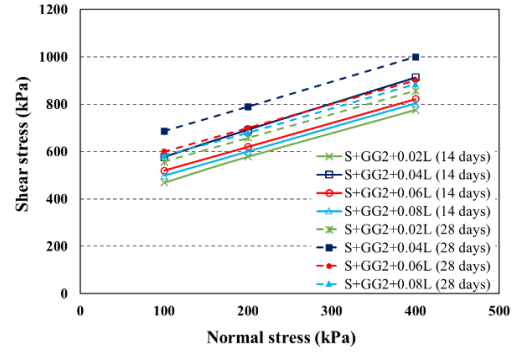

(d) GG2-reinforced at curing ages of 14 and 28 days

Fig. 5 Shear strength of geogrid-reinforced soils (lime stabilized vs. unstabilized)

This highlights the significant strengthening effect of lime stabilization. Interestingly, even without lime stabilization, reinforcing the soil with GG1 still demonstrated a 94% increase in shear strength. However, the most significant enhancement was achieved by combining both techniques. When 4% lime stabilization was applied alongside GG1 reinforcement and cured for 28 days, it resulted in 402% and 160% increase in shear strength compared to the unstabilized-unreinforced and GG1-reinforced samples, respectively. This finding suggests that the combined approach of lime stabilization and geogrid reinforcement offers a powerful strategy for significantly boosting the shear strength of cohesive soils. It is also worth noting that after GG1-reinforced specimens, reinforcement with GG2, GT2, and GT1, respectively, led to the highest increase in shear strength.

According to Fig. 8(a), the optimal lime percentage is 4% for the stabilized-unreinforced and stabilized-reinforced specimens. Furthermore, the GG1-reinforced specimen results in the highest shear strength among all unstabilized-reinforced specimens under the same conditions. According to Fig. 8(b), the shear strength improvement has a steep slope at early curing days in such a way that 80-90% of the shear strength achieved in the first 14 curing days. This phenomenon is attributed to the mechanism of lime reaction with clay particles as revealed by transmission electron microscopy and the X-ray diffraction (Al-Mukhtar *et al.* 2010, Al-Mukhtar *et al.* 2012, Al-Swaidani *et al.* 2016).

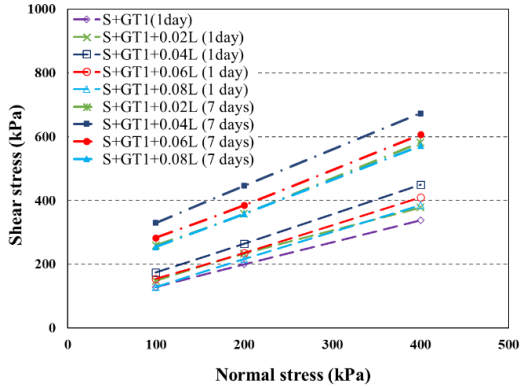

(a) GT1-reinforced at curing ages of 1 and 7 days

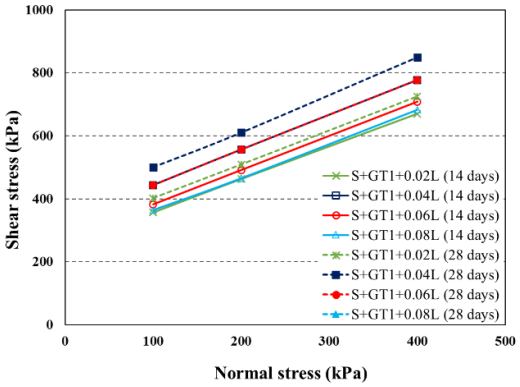

(b) GT1-reinforced at curing ages of 14 and 28 days

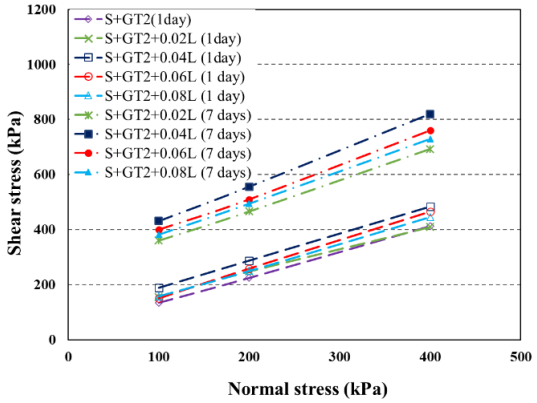

(c) GT2-reinforced at curing ages of 1 and 7 days

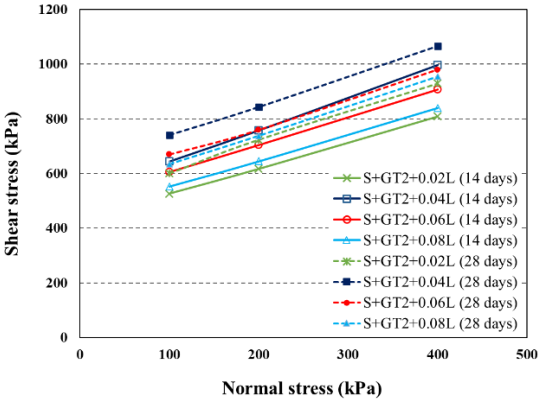

(d) GT2-reinforced at curing ages of 14 and 28 days

Fig. 6 Shear strength of geotextile-reinforced soils (lime stabilized vs. unstabilized)

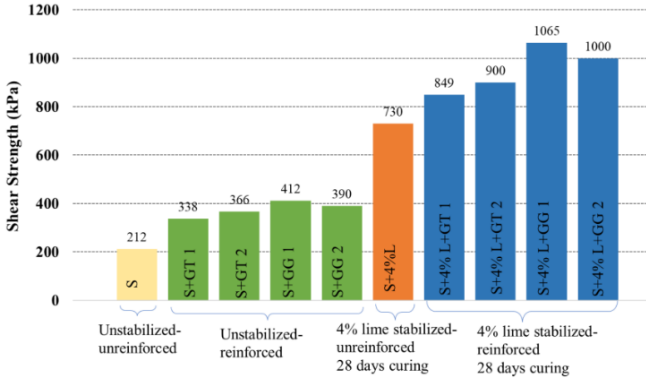

Fig. 7 Shear Strength comparison of unstabilized (reinforced and unreinforced) vs. stabilized (reinforced and unreinforced) specimens under a normal stress of 400 kPa

Lime is decomposed into Ca^{+} and OH^{-} ions once it is added to the moist soil. The released Ca^{+} ions tends to undergo ion exchange reactions with the ions in the soil, such as Na^{+} and K^{+} ions. This exchange occurs instantaneously, thus reducing the distance between clay minerals, leading to the integration of clay particles into larger particles, and showing silt and sand behavior. The remaining Ca^{+} ions react with the metal oxides, e.g., aluminates and silicates, to form calcium silicate hydrates and calcium aluminate hydrates. This strength enhancement is attributed to pozzolanic reactions. These time-dependent

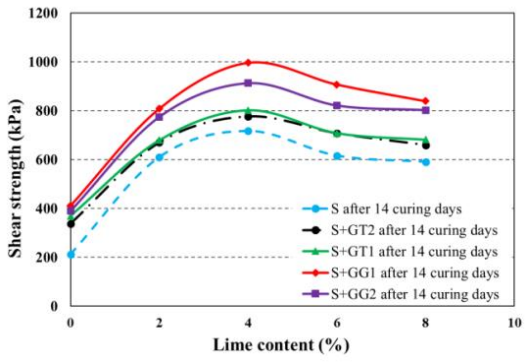

(a) Versus lime content

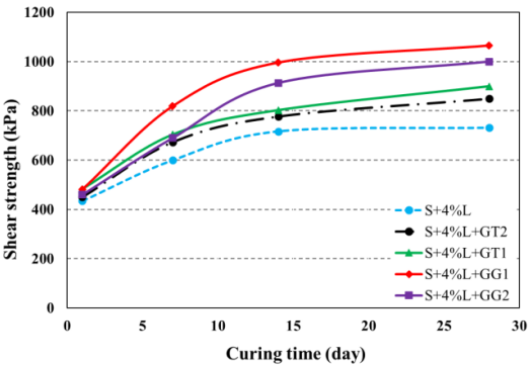

(b) Versus curing time

Fig. 8 Variation of shear strength of reinforced stabilized specimens under a normal stress of 400 kPa

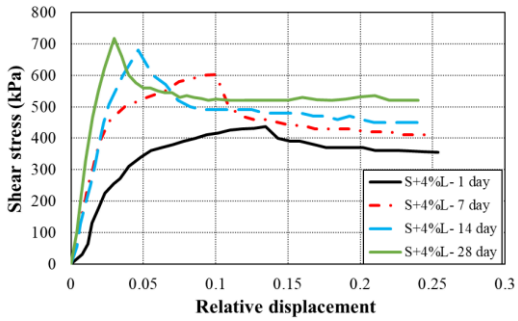

(a) Stabilized-unreinforced specimens with 4% lime and different curing ages

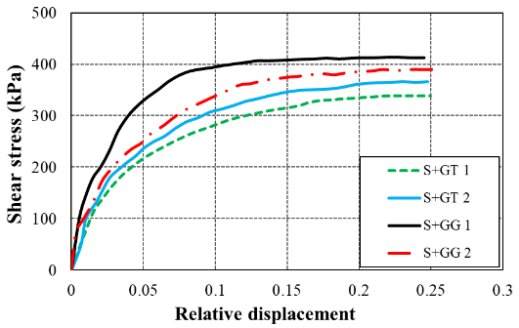

(b) Unstabilized-reinforced specimens

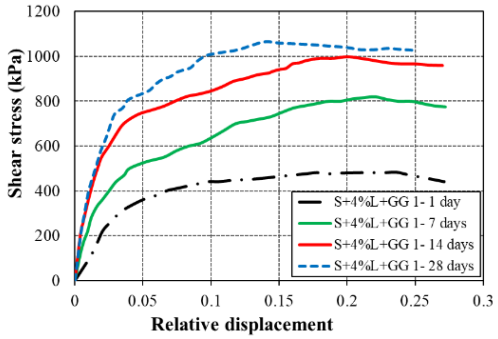

(c) GG1-reinforced/stabilized specimens with 4% lime and different curing ages

Fig. 9 Shear stress-relative displacement curve under a normal stress of 400 kPa

reactions generate an adhesive gel, which strengthens the bond between soil particles and between the soil and geosynthetic (Behnood 2018).

3.3 Brittleness index

Fig. 9 indicates the shear stress-relative displacement for various conditions. In the case of the unstabilized-reinforced and stabilized-reinforced specimens, the shear strength gently increases with the curing time to the failure point, with no certain peak. The shear strength of stabilized-unreinforced specimens; however, sharply increases to the peak, followed by a significant decrease in strength. This decline in strength can be expressed using the brittleness index, I_B, which defines based on Eq. (4) suggested by (Bishop 1971)

$$I_B = \frac{\tau_p - \tau_r}{\tau_p} \quad (4)$$

where τ_p and τ_r are the peak and residual shear strengths, respectively. Based on Eq. (4), specimens with more strength drop are more brittle. The brittleness index for stabilized-unreinforced and stabilized-reinforced specimens with 4% lime after 28 curing days are 0.28 and 0.03, respectively. For unstabilized-unreinforced and stabilized-reinforced specimens, I_B is zero. This implies that lime stabilization increases the brittleness of soil, which can be significantly reduced by geosynthetic reinforcement.

3.4 Resistance contribution assessment of soil-to-soil, soil-geogrid interface and transverse ribs

To investigate the interaction behavior between the geogrid and stabilized/unstabilized soils, specimens without transverse ribs were tested. Based on Eq. (1), the total shear strength of the geogrid-reinforced soil, R_{S+GG}, can be derived from three components (Liu *et al*. 2009):

- Shear strength of the soil in the open geogrid apertures, τ_{soil}
- Mobilized frictional resistance in the soil-geogrid interface, τ_{S-G}
- Bearing resistance of transverse ribs developed between the transverse geogrid components, R_B

τ_{soil} is obtained using the direct shear test of the unreinforced specimens. R_B can also be assessed based on the difference between the magnitude of shear strength of samples reinforced by geogrid with and without transverse ribs. Then, τ_{S-G} is calculated using Eq. (1). Contribution of each component to total shear resistance can also be evaluated. Transverse resistance contribution (β), can be assessed using Eq. (2). Similarly, based on Eq. (2), $A\rho\tau_{\text{Soil}}/R_{S+GG}$ and $A(1-\rho)\tau_{S-G}/R_{S+GG}$ are also represent the contribution of soil-to-soil and soil-geogrid interface, respectively. A sample calculation of shear strength components is explained in Appendix.

Fig. 10 shows the contributions of soil-to-soil interaction, soil-geogrid interface, and transverse ribs to the total shear resistance for GG1-reinforced specimens stabilized with different lime percentages at a vertical stress of 400 kPa. For unstabilized samples, transverse ribs exhibit the most significant contribution (47.6%). However, stabilization significantly reduces this contribution. After 28 days of curing, GG1-reinforced samples with 4% lime content show a reduction in the contribution of transverse

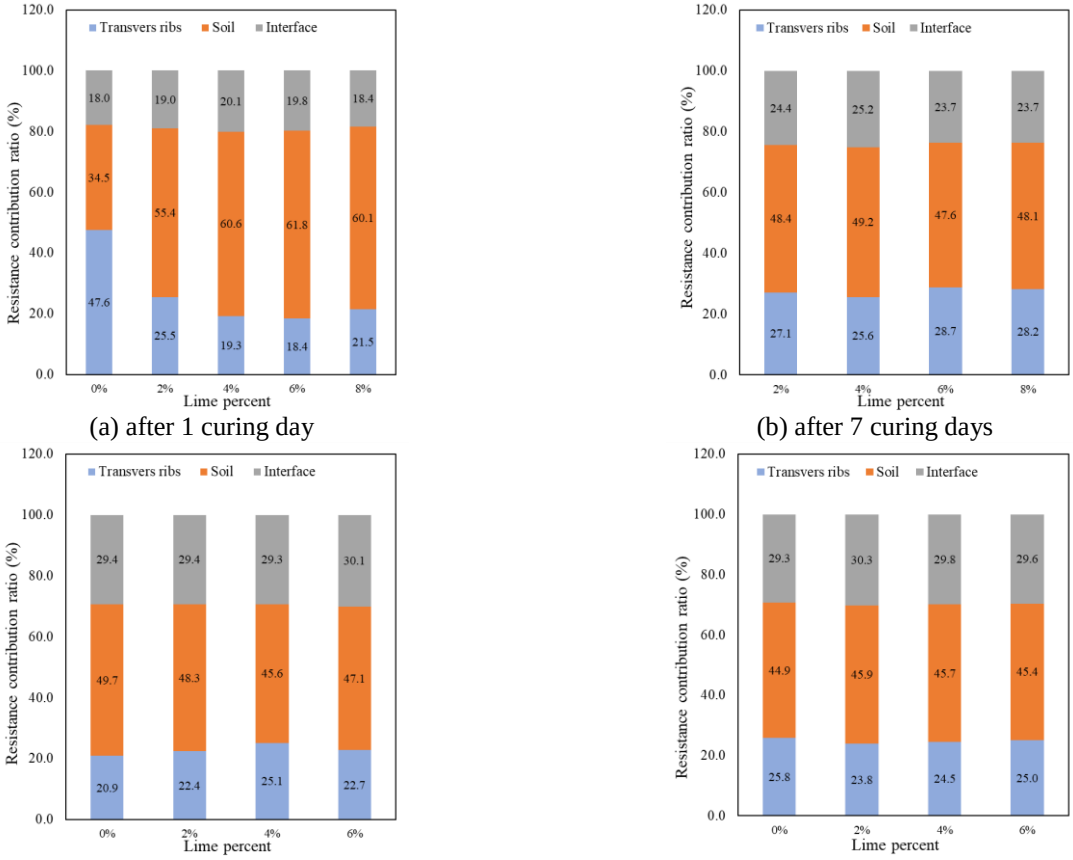

(a) after 1 curing day (b) after 7 curing days

(c) after 14 curing days (d) after 28 curing days

Fig. 10 Resistance provided by soil-to-soil, soil-geogrid interface and transverse ribs for GG1-reinforced samples (different lime percentages, normal stress 400 kPa)

ribs to 24.5%. Conversely, the contribution of soil confined within the geogrid apertures increases upon stabilization. This value rises from 34.5% before stabilization to 45.9% for soil stabilized with the optimal lime content after 28 curing days, highlighting the positive influence of stabilization on soil-to-soil resistance. The soil-geogrid interface contribution also demonstrates a rise after stabilization. While it initially stands at 18% in unstabilized samples, it increases to 30.2% for the 4% lime-stabilized sample after 28 curing days.

Fig. 11 demonstrates the contributions of soil-to-soil interaction, soil-geogrid interface, and transverse ribs to the total shear resistance for GG2-reinforced samples stabilized with different lime contents. In this case, the contribution of soil within the geogrid apertures before stabilization is 53.8%, which increases to 65.3% for the 4% lime-stabilized sample after 28 curing days. The contribution of soil-geogrid interface resistance to the total shear resistance is 31.5% before stabilization and reduces to 18.8% after stabilization with the optimal lime content after 28 curing days. Moreover, transverse ribs contribute 14.7% and 15.9% of the total shear resistance before and after stabilization, respectively.

3.5 Interaction parameters and interface efficiency

The interaction parameters of geotextile and geogrid reinforced soil stabilized with different lime contents were calculated based on τ_{S-G} values, and presented in Table 5. It can be noticed that the interaction parameters for both geogrid and geotextile show an increase after stabilization. In the case of stabilized specimens, the cohesion and friction angle of stabilized soil/geosynthetics interface increase as the lime concentration rises to the optimal percentage (i.e., 4%). Increasing the lime content beyond 4% leads to a reduction in the interaction parameters. These parameters also increase with the curing time. At curing ages longer than 7 days, the Ca values for GT2, which has a higher shear strength, are greater than those for GT1, while the δ values are similar for both geotextiles. The maximum value of interaction parameters for all geosynthetics corresponds to the specimens stabilized with the optimum lime percent at a curing time of 28 days.

The interface efficiency (C_i) is an essential parameter in the design of reinforced soil structures. Table 6 represents the interface efficiency of the reinforced specimens, calculated using Eq. (3). For unstabilized specimens, C_i for all types of geosynthetics is more than 1 which indicates interface shear resistance of geosynthetic-reinforced/unstabilized samples is greater than the shear resistance of unreinforced-unstabilized specimens. These results are consistent with previous studies (Bergado *et al.*

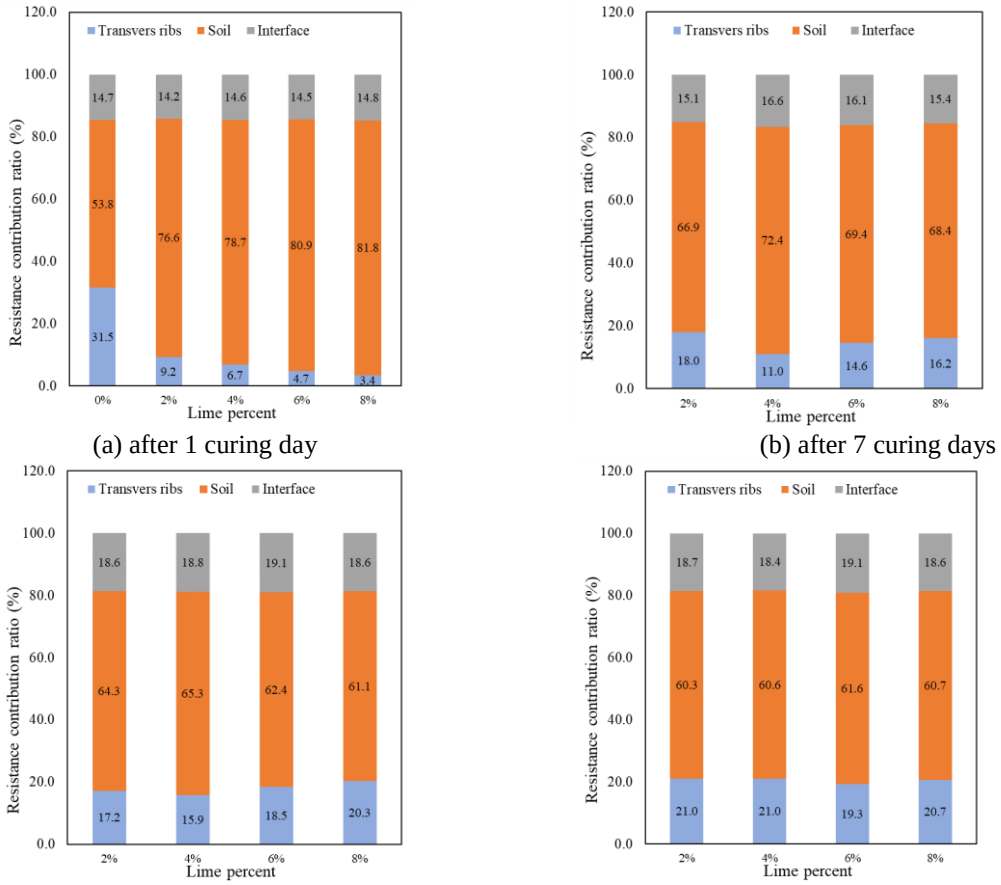

(a) after 1 curing day (b) after 7 curing days

(c) after 14 curing days (d) after 28 curing days

Fig. 11 Resistance provided by soil-to-soil, soil-geogrid interface and transverse ribs for GG2-reinforced samples (different lime percentages, normal stress 400 kPa)

1993, Hebeler and Martinez 2016, Razeghi and Ensani 2023, Chai *et al.* 2024) which can be attributed to effective soil particle interlocking between geotextile fibers and geogrid apertures. Despite this, numerous studies have also shown that the mobilized shear strength at the interface of soil-geogrid is typically lower than the soil shear strength itself (Abu-Farsakh *et al.* 2007, Arulrajah *et al.* 2014, Choudhary and Krishna 2016, Khunt *et al.* 2020). Vangla and Latha (2016) found that the roughness of the interface plays a key role for interface shear resistance achievement and quantified the surface roughness as Asperity ratio (AR)

$$AR = \frac{AS}{D_{50}} \tag{5}$$

where AS is the half asperity spacing, i.e., the half distance between two transverse ribs for geogrids and D_{50} is the mean particle size of a soil. Chai *et al*. (2024) found that a lower AR (indicating a rougher surface) typically associated with the geogrids with smaller apertures, leads to a significant increase in interface cohesion (C_a). Similarly, analysis of Tables 5 and 6 suggests that the greater interface cohesion can be attributed to geogrid with smaller apertures leading to higher interface efficiency. As a result, the geogrid with smaller aperture size is more effective for clay reinforcement, which could be led to C_i exceeding 1.

For geotextiles, C_i for GT2 and GT1-reinforced-unstabilized specimens is 1.87 and 1.67, respectively. This suggests that geotextiles create a more robust bond at the soil interface in comparison to geogrids for unstabilized samples, likely due to their higher surface roughness and the ability of soil particles to plow into the geotextile surface (Chai *et al*. 2024). However, when considering soil-to-soil interaction and the resistance provided by the transverse ribs, geogrid-reinforced samples exhibit higher overall shear resistance.

Adding lime significantly affects interaction coefficients. For geotextiles, the highest C_i is found in unstabilized specimens. This indicates that stabilization reduces interface shear strength, because soil flocculation increases particle size, resulting in a weaker interlock with the geotextile. At the same condition, the GT2-reinforced specimens have higher interface efficiency than GT1-reinforced one, since the resistive force in the soil mass during reinforcement arises from the tensile resistance of the geotextile and GT2 has greater tensile strength than GT1. This is consistent with earlier works (Anubhav and Basudhar 2010). Moreover, at a given lime content, a rise in the curing age does not significantly change the interface efficiency of the geotextile-reinforced specimens. The interface efficiency of the lime-stabilized/geogrid-reinforced specimens is lower than 1 at a curing age of 1

Table 5 Geosynthetic-soil interaction parameters

		Geosynthetic type							
		GG1		GG2		GT1		GT2	
Curing days	Lime percentage	C_a (kPa)	δ (°)	C_a (kPa)	δ (°)	C_a (kPa)	δ (°)	C_a (kPa)	δ (°)
1	0	86.8	19	10	34.3	60	34.8	57.5	39.9
	2	97.9	21	17.3	37.6	70.5	37.5	75	40.1
	4	126.8	22.6	37.3	41.7	82.5	42.5	90	44.5
	6	110.7	22	23.3	40.4	68	40.5	51	45.4
	8	89.5	21.6	19	39.8	43.5	40.5	45.5	44.1
7	2	299	28.1	141.6	45.8	147	47.3	169	47.4
	4	396.3	29.8	242.5	47	216.5	48.8	242	49
	6	319.5	29.6	195.2	46	172	48	202	48
	8	309	28.7	159	46.3	147	47.7	158.5	47.6
14	2	383.6	40	242	56.4	254.5	47	294	47.1
	4	507.4	45	359.2	58.6	332.5	49	361.5	49.8
	6	422.6	44	282.6	57.3	273.5	48.4	313	45
	8	383.8	43.7	262.2	57	255.5	48	268.5	48.2
28	2	430.5	44.7	295.3	57.7	294	48	346.5	47.4
	4	540	47.5	416.4	59.2	380.5	49.4	418	50.3
	6	489.8	45.4	340.4	59	333	48.9	384.5	48.4
	8	450.1	45	317	58.5	312	48.8	352.5	48.7

Table 6 Interface efficiency values

		Curing days	GG1	GG2	GT1	GT2
Lime percent	0%	-	1.33	1.2	1.67	1.87
	2%	1	0.86	0.82	1.08	1.18
		7	1.26	1.08	1.13	1.2
		14	1.34	1.33	1.13	1.23
		28	1.39	1.37	1.14	1.24
	4%	1	0.89	0.85	1.1	1.19
		7	1.33	1.19	1.16	1.23
		14	1.41	1.39	1.17	1.25
		28	1.42	1.41	1.18	1.26
	6%	1	0.88	0.83	1.06	1.12
		7	1.23	1.15	1.11	1.17
		14	1.39	1.37	1.14	1.2
		28	1.4	1.39	1.14	1.24
	8%	1	0.79	0.82	1	1.08
		7	1.21	1.09	1.06	1.1
		14	1.37	1.36	1.13	1.12
		28	1.39	1.37	1.13	1.23

day and increases as the curing age progresses, leading to stronger bonding between the lime stabilized soil and geogrid. It is worth to mention that C_i for geogrid-reinforced/stabilized samples exceeds that of unstabilized ones after 14 curing days. Contrary to the unstabilized specimens, interface efficiency of the geogrid-reinforced samples at longer curing ages is greater than that of the geotextile-reinforced ones. This enhancement in bonding between the soil-lime mixture and geogrid is attributed to adhesion between stabilized soil particles and geogrid,

which improves interlocking. Moreover, lime stabilization promotes flocculation and cementation, resulting in a stiffer and more cohesive soil matrix. This, in turn, can improve interaction with the geogrid and contribute to a higher C_i. It is worth mentioning that for the stabilized specimens, the interface efficiency is maximized at the optimal lime percentage (i.e., 4%).

4. ML estimation of the soil shear strength

4.1 SVM

The SVM (support vector machine) and SVR (support vector regression) algorithms are supervised machine learning algorithms. SVM is used for classification applications, while SVR is used for regression applications. Here, for a training dataset of paired data points $(x_1, y_1), (x_2, y_2), \ldots (x_l, y_l)$, where xi ∈ Rn (i = 1,2,…, l) and yi ∈ R (i = 1,2,…, l) denote features and target variable, respectively. SVR solves the optimization problem by minimizing Eq. (6) (Xue *et al.* 2014)

$$\frac{1}{2}\|w\|^2 + C_r \sum_{i=1}^{l} (\xi_i + \xi_i^*) \tag{6}$$

Subjected to

$$\begin{cases} y_i - \sum_{j=1}^{n}\sum_{i=1}^{l} w_j x_{ji} - b \le \varepsilon + \xi_i \\ \sum_{j=1}^{n}\sum_{i=1}^{l} w_j x_{ji} + b - y_i \le \varepsilon + \xi_i^* \\ \xi_i, \xi_i^* \ge 0 \end{cases} \tag{7}$$

where

$$f(x) = \sum_{j=1}^{n} w_j x_j + b \; with \; w \in R^n, b \in R \tag{8}$$

where n is the number of features, b the bias, w the weight, x the input feature vector, y the output parameter and l the number of support vectors. Here, C_r forms a trade-off between the complexity of function f and the allowable error. Errors below ε are acceptable in SVR. Once the error exceeds ε, virtual variables ξ_i and ξ_i^* implement a penalty.

4.2 ANN

An ANN (artificial neural network) is a powerful machine learning algorithm inspired by the human brain. It consists of an input layer, an output layer, and one or more hidden layers. These layers contain interconnected neurons. The neurons in the input layer receive the input data. The data points are multiplied by the corresponding weights and summed with a bias (Eq. (9)). Then, the activation function, *f,* is applied to the data, obtaining the output. This process is performed in all the next layers until the output of the model is generated.

Table 7 Statistical parameters of the dataset

Features	Variable	Mean	Std	Min	Max
Lime percent	Input	4.7	2.5	0	8
Curing days	Input	11.8	10.1	1	28
Moisture content	Input	18.5	1.0	15.3	19.4
Vertical stress (kpa)	Input	233.3	124.9	100	400
Shear strength (kpa)	Output	459.4	208.2	73	1065

$$y=f(wx+b) \tag{9}$$

where *x* is the input data vector, *w* the weight vector, *b* the bias, f the activation function, and *y* the output (Theobald, 2017).

This study employed SVM and ANN algorithms to estimate the shear strength of stabilized reinforced soils based on the experimental test data. The features included the lime content, geosynthetic type, curing age, moisture content, and normal stress. Table 7 summarizes the dataset. To obtain a reliable estimation, the hyperparameters of algorithms were tuned using the training data as described in section 4.3.

4.3 Tuning of hyperparameters

The performance and accuracy of every ML model are dependent on several factors. To maximize ML performance, it is required to find and optimize the hyperparameters. This optimization process is called hyperparameter tuning. This study adopts the grid search algorithm, where a set of possible values for each hyperparameter is defined. All possible combinations of these values are evaluated to identify the optimal combination (Brownlee 2016).

The k-fold cross-validation method was used to reduce overfitting during hyperparameter tunning (Brownlee 2016). The data were divided into *k* subsets. The algorithm was trained on *k*-1 folds, with the remaining fold being used for testing. This process is iterated *k* times leading to *k* performance scores in each stage, which are often summarized in the form of the mean and standard deviation. This approach leads to high accuracy because the model is trained several times upon different training datasets. To implement the algorithm, the dataset was divided into a training dataset (2/3 of the data) and a testing dataset (1/3 of the data). Then, 10-fold cross-validation was utilized for the training data, i.e., the training data samples were divided into ten folds, each time using one of the ten folds as the testing dataset and the remaining nine as the training dataset. No fold was used for testing more than once. Therefore, an optimal combination of SVM and ANN hyperparameters was found for the shear strength estimation of the stabilized reinforced soils. Fig. 12 depicts the procedure. It should be noted that the training and testing datasets consisted of 239 and 118 data samples, respectively.

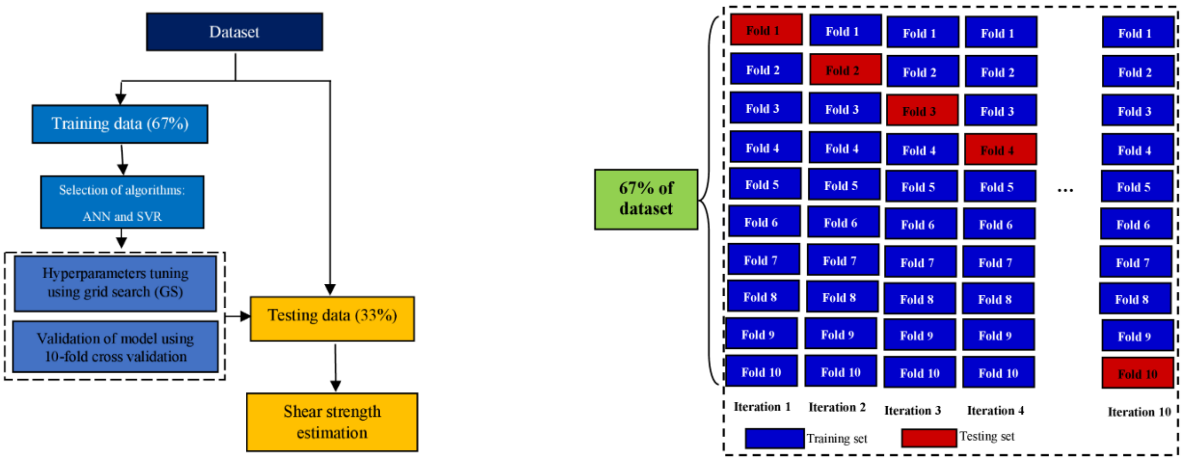

(a) Procedure (b) Hyperparameter tuning

Fig. 12 ML methodology

Table 8 SVM and ANN hyperparameter tuning

Algorithm	Selected hyperparameters for tuning	The range of variation for each hyperparameters	Best results from grid search
ANN	Hidden_layer_sizes	From 5 to 250 with increments of 5	200
	Activation function	logistic, tanh, relu	tanh
	Solver	lbfgs, sgd, adam	lbfgs
SVM	Regularization parameter (C_r)	From 5 to 100 with increments of 5	10
	Gamma	scale, auto	scale
	Kernel	linear, poly, rbf, sigmoid	rbf

The tuned hyperparameters of the SVR algorithm included the kernel type, regularization parameter (C_r), and gamma. A larger regularization parameter requires an error of almost zero, which makes it impossible to solve many problems. On the other hand, an excessively small regularization parameter reduces the intensity of constraints and raises errors. The optimal regularization parameter enables the model to find the optimal response at a reasonable error. To solve nonlinear problems, SVR maps the data into the linear space via nonlinear kernels. Radial Basis Functions (RBFs) are popular kernels, in which gamma plays a key role in data mapping into the linear space. For the ANN model, one hidden layer was used, and the hidden layer size, activation function, and solver were tuned. Table 8 represents the hyperparameter tunning method for SVR and ANN algorithms.

4.4 Performance evaluation

The performance of the ANN and SVM models in the shear strength estimation of stabilized reinforced soils was evaluated using the Root-Mean-Square Error (RMSE) and coefficient of determination (R^2). Figs. 13(a) and 13(b) plot predicted shear strength values of SVM and ANN versus the experimental data in the training dataset, respectively.

The 10-fold cross-validation technique was employed to obtain these estimates for the training dataset, using the mean results. The coefficient of determination is found to be greater than 0.99 for both the ANN and SVM algorithms, suggesting superior performance in the training dataset. Figs. 14(a) and 14(b) describe the shear strength estimates

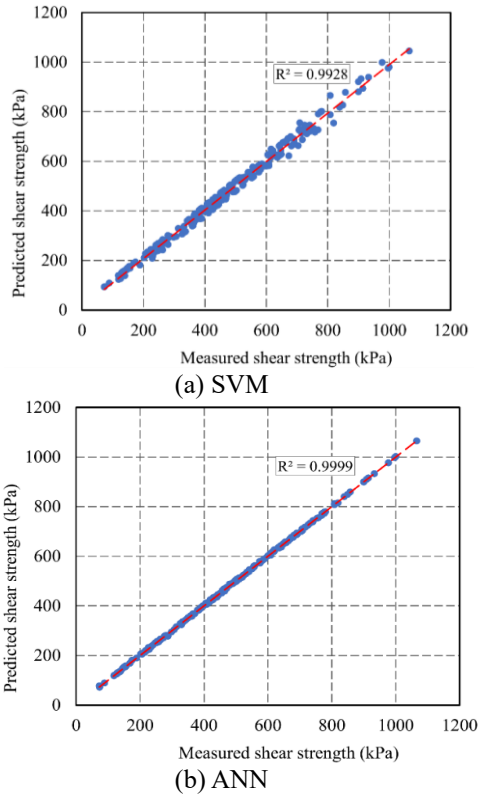

(a) SVM

(b) ANN

Fig. 13 Performance evaluation on the training dataset

of SVM and ANN versus the experimental data in the testing dataset, respectively. The coefficient of determination is calculated to be 0.98 for SVM and 0.99 for

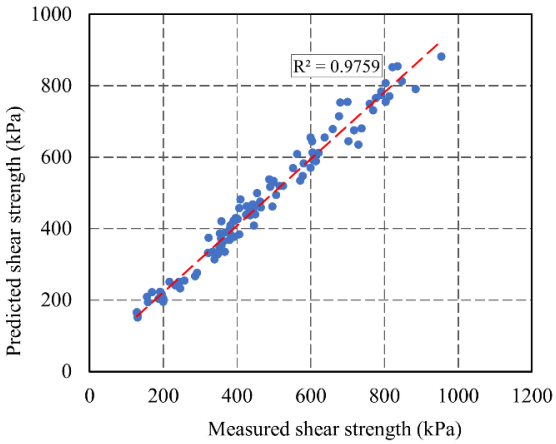

(a) SVM

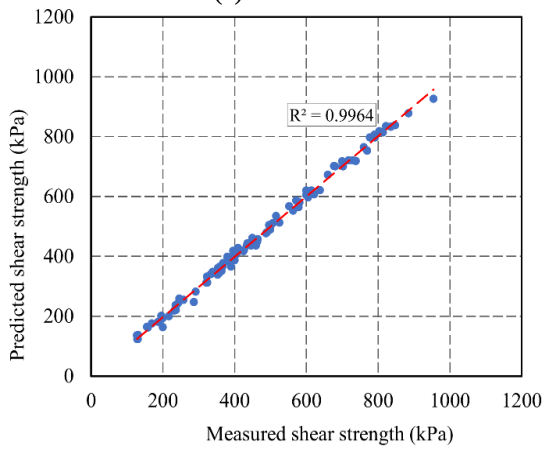

(b) ANN

Fig. 14 Performance evaluation in the testing dataset

ANN, suggesting that these models were effectively trained. The RMSE is found to be 0.061 and 0.158 for the ANN and SVM algorithms, respectively, suggesting that ANN is more accurate than SVM in this study. These results are in accordance with the findings of Kanungo *et al.* (2014) and Pham *et al.* (2018) which support the potential of the ANN and SVM as a reliable approach for predicting soil shear strength, respectively.

For the investigation of the contribution of the input variables to the shear strength, sensitivity analysis was performed. The sensitivity percentage (S_i) is determined using the Eq. (10) (Gandomi *et al.* 2013)

$$N_i = f_{max}(x_i) - f_{min}(x_i) \quad (10a)$$

$$S_i = \frac{N_i}{\sum_{j=1}^{n} N_j} \times 100 \quad (10b)$$

in which, x is the input feature, n the number of features, $f_{max}(x_i)$ and $f_{min}(x_i)$ are respectively the maximum and minimum values of shear strength over the *i*th input variable, while all other variables are set to their average values. A higher Si value indicates that the variable has a greater influence on the shear strength; it is important to note that in this method the sum of all Si values is always 100. Sensitivity analysis results in Fig. 15 show that lime stabilization, geosynthetic reinforcement, moisture content, curing days, and vertical stress have the highest

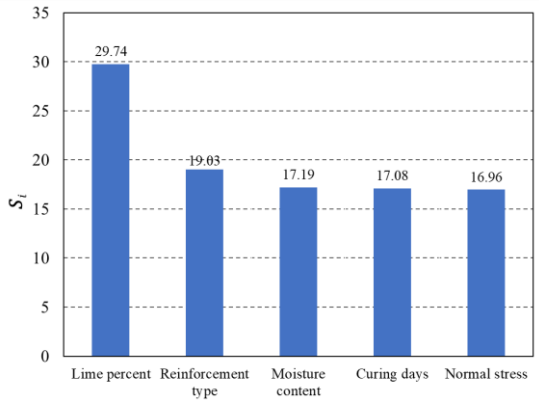

Fig. 15 Sensitivity analysis results

contributions to the soil shear strength achievement, respectively. By quantifying the contribution of each variable through sensitivity analysis, researchers can make more informed decisions about soil stabilization and reinforcement strategies.

5. Conclusions

This study investigated the effects of lime stabilization on the shear strength and interface characteristics of geosynthetic-reinforced soil specimens. The interaction parameters and interface efficiency (C_i) were evaluated using the direct shear test results at different lime percentages for both stabilized and unstabilized conditions. Additionally, machine learning algorithms (SVM and ANN) were employed to estimate the shear strength of reinforced stabilized soil. The following key findings were extracted from this study:

- Lime stabilization significantly increased the shear strength of the clayey soil. The optimum lime content for both unreinforced and geosynthetic-reinforced specimens was 4%. However, stabilization also led to an increase in brittleness, which can be mitigated by geosynthetic reinforcement.
- Geosynthetic reinforcement increased the shear strength of the specimens. However, its contribution was less significant than lime stabilization to the enhancement of shear strength. Geogrids demonstrated superior performance in enhancing shear strength compared to geotextiles.
- For geogrid-reinforced specimens, the total shear resistance consists of three components: soil resistance within the geogrid apertures, soil-geogrid interface resistance, and transverse rib resistance. Stabilization with lime had a differential effect on these contributions depending on the geogrid type. For GG1 (smaller aperture), stabilization increased soil-to-soil and soil-interface contributions while decreasing transverse rib contribution. Conversely, for GG2 (larger aperture), stabilization decreased the interface contribution and increased the contribution of soil and transverse ribs. Regardless of the geogrid type, soil in

geogrid apertures always exhibited higher contribution to shear resistance after stabilization.

- The shear strength parameters (C_a and δ) of the geosynthetic-stabilized soil interface exhibited a positive correlation with curing time, reaching a maximum at the optimum lime content. These values surpassed those of the unstabilized soil after 7 days of curing.
- The interface efficiency (C_i) of unstabilized specimens was initially higher for geotextiles compared to geogrids. After stabilization, C_i decreases sharply for all reinforcements but gradually increases with curing time. Notably, the maximum C_i for geotextiles after stabilization was lower than the unstabilized state. Conversely, geogrids (GG1 and GG2) displayed an increase in C_i after stabilization compared to the unstabilized condition. Overall, the C_i values were greater than 1, indicating a strong bond between the geosynthetics and the soil.
- Under the same conditions, geotextile-reinforced samples with a higher tensile strength (GT2) displayed a greater C_i . Additionally, GG1-reinforced samples have a greater C_i than the GG2-reinforced samples under similar conditions, suggesting that geogrid with smaller apertures is more efficient for fine-grained soil reinforcement. However, geogrids with such small apertures are uncommon in practice. Further studies by employing large direct shear test could explore the utilization of geogrids with larger apertures.
- Both SVM and ANN algorithms demonstrated excellent performance in predicting the shear strength of reinforced stabilized soil, with R^2 values exceeding 0.98. These models can provide a reliable initial estimate of shear strength for geotechnical design applications, potentially reducing the need for extensive direct shear testing. Additionally, the sensitivity analysis results show that among the input parameters, lime percentage and, to a lesser extent, the reinforcement type are the most effective parameters in achieving soil shear strength.

References

Abdi, M.R., Ghalandarzadeh, A. and Shafiei Chafi, L. (2021), "An investigation into the effects of lime on compressive and shear strength characteristics of fiber-reinforced clays", *J. Rock Mech. Geotech. Eng.*, **13**(4), 885-898. https://doi.org/10.1016/j.jrmge.2020.11.008.

Abu-Farsakh, M., Coronel, J. and Tao, M. (2007), "Effect of soil moisture content and dry density on cohesive soil–geosynthetic interactions using large direct shear tests", *J. Mater. civil Eng.*, **19**(7), 540-549. https://doi.org/10.1061/(ASCE)0899-1561(2007)19:7(540).

Al-Mukhtar, M., Khattab, S. and Alcover, J.F. (2012), "Microstructure and geotechnical properties of lime-treated expansive clayey soil", *Eng. Geol.*, **139**, 17-27. https://doi.org/10.1016/j.enggeo.2012.04.004.

Al-Mukhtar, M., Lasledj, A. and Alcover, J.F. (2010), "Behaviour and mineralogy changes in lime-treated expansive soil at 20 C", *Appl. Clay Sci.*, **50**(2), 191-198. https://doi.org/10.1016/j.clay.2010.07.023.

Al-Swaidani, A., Hammoud, I. and Meziab, A. (2016), "Effect of adding natural pozzolana on geotechnical properties of lime-stabilized clayey soil", *J. Rock Mech. Geotech. Eng.*, **8**(5), 714-725. https://doi.org/10.1016/j.jrmge.2016.04.002.

Armaghani, D.J., Mirzaei, F., Shariati, M., Trung, N.T., Shariati, M. and Trnavac, D. (2020), "Hybrid ANN-based techniques in predicting cohesion of sandy-soil combined with fiber", *Geomech. Eng.*, **20**(3), 191-205. https://doi.org/10.12989/gae.2020.20.3.191.

Arulrajah, A., Rahman, M.A., Piratheepan, J., Bo, M.W. and Imteaz, M.A. (2014), "Evaluation of Interface Shear Strength Properties of Geogrid-Reinforced Construction and Demolition Materials Using a Modified Large-Scale Direct Shear Testing Apparatus", *J. Mater. Civil Eng.*, **26**(5), 974-982. https://doi.org/10.1061/(asce)mt.1943-5533.0000897.

ASTM D- 3080. (2003), *Standard test method for direct shear test of soils under consolidated drained conditions*, Annual book of ASTM standards; 4(8) United States.

ASTM D- 5321. (2014), *Standard test method for determining the shear strength of soil-geosynthetic and geosynthetic-geosynthetic interfaces by direct shear*, United States.

Basudhar, P.K. (2010), "Modeling of soil–woven geotextile interface behavior from direct shear test results", *Geotext. Geomembranes*, **28**(4), 403-408. https://doi.org/10.1016/j.geotexmem.2009.12.005.

Behnood, A. (2018), "Soil and clay stabilization with calcium- and non-calcium-based additives: A state-of-the-art review of challenges, approaches and techniques", *Transport. Geotech.*, **17**, 14-32. https://doi.org/10.1016/j.trgeo.2018.08.002.

Bell, F. (1996), "Lime stabilization of clay minerals and soils", *Eng. Geol.*, **42**(4), 223-237. https://doi.org/10.1016/0013-7952(96)00028-2.

Bergado, D., Chai, J., Abiera, H., Alfaro, M. and Balasubramaniam, A. (1993), "Interaction between cohesive-frictional soil and various grid reinforcements", *Geotext. Geomembranes*, **12**(4), 327-349. https://doi.org/10.1016/0266-1144(93)90008-C.

Bishop, A.W. (1971), "Shear strength parameters for undisturbed and remolded soil specimens", *Roscoe Memorial Symposium*, Cambridge.

Bozbey, I., Kelesoglu, M.K., Demir, B., Komut, M., Comez, S., Ozturk, T., Mert, A., Ocal, K. and Oztoprak, S. (2018), "Effects of soil pulverization level on resilient modulus and freeze and thaw resistance of a lime stabilized clay", *Cold Reg. Sci. Technol.*, **151**, 323-334. https://doi.org/10.1016/j.coldregions.2018.03.023.

Brownlee, J. (2016), *Machine learning mastery with Python: understand your data, create accurate models, and work projects end-to-end*, Machine Learning Mastery.

Cai, Y., Shi, B., Ng, C.W. and Tang, C.S. (2006), "Effect of polypropylene fibre and lime admixture on engineering properties of clayey soil", *Eng. Geol.*, **87**(3), 230-240. https://doi.org/10.1016/j.enggeo.2006.07.007.

Chai, J.C., Saito, A. and Hino, T. (2024), "Effect of Surface Roughness on Soil-Geogrid/Geotextile Interface Shear Strengths", *Int. J. Geosynth. Ground Eng.*, **10**. https://doi.org/10.1007/s40891-024-00558-y.

Choudhary, A.K. and Krishna, A.M. (2016), "Experimental Investigation of Interface Behaviour of Different Types of Granular Soil/Geosynthetics", *Int. J. Geosynth. Ground Eng.*, **2**(1), 1-11. https://doi.org/10.1007/s40891-016-0044-8.

Cowell, M. (1993), "Comparison of pull-out performance of geogrids and geotextiles", *Proceedings of Geosynthetics*, Roseville.

Dash, S.K. and Hussain, M. (2012), "Lime stabilization of soils: reappraisal", *J. Mater. Civil Eng.*, **24**(6), 707-714.

Dinarvand, R. and Ardakani, A. (2022), "Shear behavior of geotextile-encased gravel columns in silty sand-Experimental and SVM modeling", *Geomech. Eng.*, **28**(5), 505-520. https://doi.org/10.12989/gae.2022.28.5.505.

Gandomi, A.H., Yun, G.J. and Alavi, A.H. (2013), "An evolutionary approach for modeling of shear strength of RC deep beams", *Mater. Struct*., **46**, 2109-2119. https://doi.org/10.1617/s11527-013-0039-z.

Ghanizadeh, A.R., Heidarabadizadeh, N., Bayat, M. and Khalifeh, V. (2022), "Modeling of unconfined compressive strength and Young's modulus of lime and cement stabilized clayey subgrade soil using Evolutionary Polynomial Regression (EPR)", *Int. J. Min. Geo-Eng*., https://doi.org/10.22059/IJMGE.2022.306688.594858.

Guney, Y., Sari, D., Cetin, M. and Tuncan, M. (2007), "Impact of cyclic wetting–drying on swelling behavior of lime-stabilized soil", *Build. Environ.*, **42**(2), 681-688. https://doi.org/10.1016/j.buildenv.2005.10.035.

Hebeler, G.L., Martinez, A. and Frost, J.D. (2016), "Shear zone evolution of granular soils in contact with conventional and textured CPT friction sleeves", *KSCE J. Civil Eng*., **20**(4), 1267-1282. https://doi.org/10.1007/s12205-015-0767-6.

Jahandari, S., Saberian, M., Zivari, F., Li, J., Ghasemi, M. and Vali, R. (2019), "Experimental study of the effects of curing time on geotechnical properties of stabilized clay with lime and geogrid", *Int. J. Geotech. Eng.*, **13**(2), 172-183. https://doi.org/10.1080/19386362.2017.1329259.

Jalal, F.E., Xu, Y., Iqbal, M., Javed, M.F. and Jamhiri, B. (2021), "Predictive modeling of swell-strength of expansive soils using artificial intelligence approaches: ANN, ANFIS and GEP", *J. Environ. Management*, **289**, 112420. https://doi.org/10.1016/j.jenvman.2021.112420.

Kanungo, D.P., Sharma, S. and Pain, A. (2014), "Artificial neural network (ANN) and regression tree (CART) applications for the indirect estimation of unsaturated soil shear strength parameters", *Front. Earth Sci.*, **8**(3), 439-456. https://doi.org/10.1007/s11707-014-0416-0.

Khunt, S., Kantesaria, N., and Sachan, A. (2020), "Interface shear strength behaviour of marginal soils with geotextiles and geogrids", *Proceedings of the Geo-Congress 2020*, February.

Kumar, A., Walia, B.S. and Abjaj, A. (2007), "Influence of fly ash, lime, and polyester fibers on compaction and strength properties of expansive soil", *J. Mater. Civil Eng.*, **19**(3), 242-248.

Lin, P., Chen, X., Jiang, M., Song, X., Xu, M. and Huang, S. (2022), "Mapping shear strength and compressibility of soft soils with artificial neural networks", *Eng. Geol.*, **300**, 106585. https://doi.org/10.1016/j.enggeo.2022.106585.

Liu, C.N., Ho, Y.H. and Huang, J.W. (2009), "Large scale direct shear tests of soil/PET-yarn geogrid interfaces", *Geotext. Geomembranes*, **27**(1), 19-30. https://doi.org/10.1016/j.geotexmem.2008.03.002.

Lopes, M.L. (2002), *Soil–Geosynthetic Interaction*, *Geosynthetics and Their Applications*. Thomas Telford Publishing.

Marienfeld, M.L. (2013), "Geosynthetics and common sense give you design options", *Airfield and Highway Pavement*, Los Angeles, June.

Okonta, F.N. and Nxumalo, S.P. (2022), "Strength properties of lime stabilized and fibre reinforced residual soil", *Geomech. Eng.*, **28**(1), 35-48. https://doi.org/10.12989/gae.2022.28.1.035.

Pham, B.T., Son, L.H., Hoang, T.A., Nguyen, D.M. and Tien Bui, D. (2018), "Prediction of shear strength of soft soil using machine learning methods", *CATENA*, **166**, 181-191. https://doi.org/10.1016/j.catena.2018.04.004.

Porbaha, A. (1996), "Geotextile reinforced lime treated cohesive soil retaining walls", *Geosynth. Int.*, **3**(3), 393-405. https://doi.org/10.1680/gein.3.0068.

Pramanik, R., Mukherjee, S. and Sivakumar Babu, G. (2022), "Probabilistic assessment of geosynthetic reinforced soil walls using ANN-based response surface method", *Georisk: Assessment and Management of Risk for Engineered Systems and Geohazards*, 1-23. https://doi.org/10.1080/17499518.2022.2046790.

Ramesh, H., Kulkarni, M.G.R., Raghunandan, M.E. and Nethravathi, S. (2022), "Suitability of bagasse ash-lime mixture for the stabilization of black cotton soil", *Geomech. Eng.*, **28**(3), 255-263. https://doi.org/10.12989/gae.2022.28.3.255.

Rastegarnia, A., Alizadeh, S.M.S., Esfahani, M.K., Amini, O. and Utyuzh, A.S. (2020), "The effect of hydrated lime on the petrography and strength characteristics of Illite clay", *Geomech. Eng.*, **22**(2), 143-152. https://doi.org/10.12989/gae.2020.22.2.143.

Razeghi, H.R., and Ensani, A. (2023), "Clayey sand soil interactions with geogrids and geotextiles using large-scale direct shear tests", *Int. J. Geosynthetics Ground Eng*., **9**(2), 24. https://doi.org/10.1007/s40891-023-00443-0.

Roodi, G.H. and Zornberg, J.G. (2020), "Long-term field evaluation of a geosynthetic-stabilized roadway founded on expansive clays", *J. Geotech. Geoenviron. Eng.*, **146**(4), 05020001. https://doi.org/10.1061/(ASCE)GT.1943-5606.0002206.

Saeed, K.A.H., Kassim, K.A., Yunus, N.Z.M. and Nur, H. (2015), "Physico-chemical characterization of lime stabilized tropical kaolin clay", *J. Teknologi*, **72**(3). https://doi.org/10.11113/jt.v72.4021.

Selvakumar, S. and Soundara, B. (2019), "Swelling behaviour of expansive soils with recycled geofoam granules column inclusion", *Geotext. Geomembranes*, **47**(1), 1-11. https://doi.org/10.1016/j.geotexmem.2018.08.007.

Stoltz, G., Cuisinier, O. and Masrouri, F. (2014), "Weathering of a lime-treated clayey soil by drying and wetting cycles", *Eng. Geol.*, **181**, 281-289. https://doi.org/10.1016/j.enggeo.2014.08.013.

Sujatha, E.R., Geetha, A., Jananee, R. and Karunya, S. (2018), "Strength and mechanical behaviour of coir reinforced lime stabilized soil", *Geomech. Eng.*, **16**(6), 627-634.

Suman, S., Mahamaya, M. and Das, S.K. (2016), "Prediction of maximum dry density and unconfined compressive strength of cement stabilised soil using artificial intelligence techniques", *Int. J. Geosynth. Ground Eng.*, **2**(2), 11. https://doi.org/10.1007/s40891-016-0051-9.

Tabarsa, A., Latifi, N., Osouli, A. and Bagheri, Y. (2021), "Unconfined compressive strength prediction of soils stabilized using artificial neural networks and support vector machines", *Front. Struct. Civil Eng.*, **15**(2), 520-536. https://doi.org/10.1007/s11709-021-0689-9.

Tang, C., Shi, B., Gao, W., Chen, F. and Cai, Y. (2007), "Strength and mechanical behavior of short polypropylene fiber reinforced and cement stabilized clayey soil", *Geotext. Geomembranes*, **25**(3), 194-202. https://doi.org/10.1016/j.enggeo.2014.08.013.

Tatlisoz, N., Edil, T.B. and Benson, C.H. (1998), "Interaction between reinforcing geosynthetics and soil-tire chip mixtures", *J. Geotech. Geoenviron. Eng*., **124**(11), 1109-1119. https://doi.org/10.1061/(ASCE)1090-0241(1998)124:11(1109).

Theobald, O. (2017), *Machine Learning for Absolute Beginners: A Plain English Introduction*, Scatterplot press,

Tiwari, N. and Satyam, N. (2020), "An experimental study on the behavior of lime and silica fume treated coir geotextile reinforced expansive soil subgrade", *Eng. Sci. Technol. Int. J*., **23**(5), 1214-1222. https://doi.org/10.1016/j.jestch.2019.12.006.

Vangla, P. and Gali, M.L. (2016), "Effect of particle size of sand and surface asperities of reinforcement on their interface shear

behaviour", *Geotext. Geomembranes*, **44**(3), 254-268. https://doi.org/10.1016/j.geotexmem.2015.11.002.
Wang, D., Abriak, N.E., Zentar, R. and Chen, W. (2013), "Effect of lime treatment on geotechnical properties of Dunkirk sediments in France", *Road Mater. Pavement Design*, **14**(3), 485-503. https://doi.org/10.1080/14680629.2012.755935.
Xue, X., Yang, X. and Chen, X. (2014), "Application of a support vector machine for prediction of slope stability", *Sci. China Technol. Sci.*, **57**(12), 2379-2386. https://doi.org/10.1007/s11431-014-5699-6.
Ye, B., Ye, G., Nagaya, J. and Sugano, T. (2012), "Numerical simulation of shaking-table tests on soil-stabilized, geosynthetic-reinforced quay-wall structures", *Geosynth. Int.*, **19**(1), 54-61. https://doi.org/10.1680/gein.2012.19.1.54.

CC

Appendix: Sample calculation of shear strength components for GG1-reinforced specimen

This section presents a sample calculation of the contributions of transverse ribs, soil-to-soil interaction, and the interface to the total shear strength (τ_{S+GG}) of a GG1-reinforced specimen stabilized with 4% lime after 28 curing days under a normal stress of 400 kPa.

$Total\ shear\ strength$: $\tau_{S+GG} = 1066\ kPa$ (Fig. 5)

$Soil\ shear\ strength$: $\tau_{soil} = 730\ kPa$ (Fig. 4)

$\tau_{S+GG}(without\ transverse\ ribs) = 812\ kPa$

$A = 6 \times 6 = 36\ cm^2$ (Direct shear box area)

Percent open area: $\rho = 0.67$ (Table 3)

Calculations of interface shear strength (τ_{S-G}) based on Eq. (1)

$$R_{S+GG} = A.\rho.\tau_{soil} + A(1-\rho)\tau_{S-G} + R_B \quad (1)$$

$$1066 \times 0.0036 = (0.0036 \times 0.67) \times (730) + (1-0.67)0.0036 \times \tau_{S-G} + (1066 - 812)$$

$\tau_{S-G} = 978.5$ kPa

Transverse ribs contribution (Eq. (2))

$$\beta = (R_{S+GG} - A.\rho.\tau_{soil} - A(1-\rho)\tau_{S-G})/R_{S+GG} \quad (2)$$

$$\beta = \frac{1066 \times 0.0036 - 0.0036 \times 0.67 \times 730 - 0.0036(1-0.67)978.5}{1066 \times 0.0036} = 0.24$$

Soil-to-soil contribution:

$$A.\rho.\frac{\tau_{soil}}{R_{S+GG}} = 0.0036 \times 0.67 \times \frac{730}{1066 \times 0.0036} = 0.46$$

Interface contribution:

$$A.(1-\rho).\frac{\tau_{S-G}}{R_{S+GG}} = 0.0036 \times (1-0.67) \times \frac{978.5}{1066 \times 0.0036} = 0.3$$

Notations

ML	Machine learning
ANN	Artificial neural network
SVM	Support vector machine
SVR	Support vector regression
RMSE	Root mean square error
R^2	Coefficient of determination
GG1	Geogrid type 1
GG2	Geogrid type 2
GT1	Geotextile type 1
GT2	Geotextile type 2
A	Total area of the shear box
ρ	Ratio of the geogrid opening area to the total shear area
R_{S+GG}	Total shear resistance of reinforced samples
R_B	Shear resistance of the transverse ribs
τ_{soil}	Soil shear resistance
τ_{S-G}	Soil-geosynthetic interface shear resistance
β	Transverse ribs contribution ratio
δ	Friction angle of the soil-reinforcement interface
C_a	Cohesion of the soil-reinforcement interface
C_i	Interface efficiency
C	Soil cohesion
φ	Soil internal friction angle
σ_n	Normal stress
I_B	Brittleness index
τ_p	Peak shear strength
τ_r	Residual shear strength
w	Weight vector
C_r	Regularization parameter
$\xi\ and\ \xi^*$	Slack variables
l	Number of support vectors
b	Bias
x	Input feature vector
y	Output parameter
n	Number of features (length of vector x)
ε	A threshold for acceptable errors
S_i	Sensitivity (%)